International Journal of Solids and Structures 47 (2010) 2775–2783

Contents lists available at ScienceDirect

International Journal of Solids and Structures

journal homepage: www.elsevier.com/locate/ijsolstr

Rate-dependent domain spacing in a stretched NiTi strip

Y.J. He, Q.P. Sun *

Department of Mechanical Engineering, The Hong Kong University of Science and Technology, Clear Water Bay, Hong Kong, China

ARTICLE INFO

Article history:
Received 11 January 2010
Received in revised form 13 May 2010
Available online 15 June 2010

Keywords:
Rate-dependent domain spacing
Power-law scaling
Thermo-mechanical coupling
Martensitic phase transition
NiTi polycrystalline shape memory alloy
Self-organized domains

ABSTRACT

Superelastic fine-grained Nickel–Titanium (NiTi) polycrystalline shape memory alloys under tensile loading deform collectively via the nucleation and growth of macroscopic martensite domains. Recent experiments on a stretched NiTi strip showed that the number of nucleated domains (or the domain spacing) increased (decreased) with increasing applied stretching rate. It is also shown that the rate dependence of the domain formation is due to the coupling between the transfer of the locally released heat and the temperature dependence of the transformation stress. In this paper, a simple one-dimensional model is developed to quantify this effect of thermo-mechanical coupling on the observed domain spacing. Analytical relationship between the domain number, thermo-mechanical properties of the material, heat transfer boundary conditions and the externally applied strain rate is established. It is found that for the case of strong heat convection the domain spacing is inversely proportional to the applied stretching rate, while for the case of weak convection, the domain spacing is dictated by a power-law scaling with exponent −0.5. The latter theoretical prediction agrees well quantitatively with the experimental data in stagnant air.

1. Introduction

NiTi polycrystalline shape memory alloys (SMA) have many applications due to their superelastic and shape memory properties, which originate from the thermoelastic martensitic phase transition of the material (Delaey et al., 1974; Abeyaratne and Knowles, 1993; Shaw et al., 2008). Stress-induced phase transition of the polycrystal consists of heterogeneous discrete events of nucleation and growth of micro-domains at the grain-size level and involves intrinsic material instability and dissipative evolution of these domains (Muller and Villaggio, 1977; Brinson et al., 2004; Puglisi and Truskinovsky, 2005; Sun and He, 2008). For fine-grained polycrystalline NiTi under tensile loading, these micro-domains can collectively form macroscopic domains. It was observed in many experiments (Shaw and Kyriakides, 1995; Shaw and Kyriakides, 1997; Shaw and Kyriakides, 1998; Li and Sun, 2002; Sun and Li, 2002; Pieczyska et al., 2004; Feng and Sun, 2006; Ng and Sun, 2006; He and Sun, 2009a,b; Churchill et al., 2009 among many others) that polycrystalline NiTi strips/wires/tubes under stretching deform via the nucleation and growth of macroscopic martensite domains which consists of almost fully-transformed grains. Detailed experiments (Shaw and Kyriakides, 1995; Shaw and Kyriakides, 1997; Ng and Sun, 2006; Pieczyska et al., 2006; Zhang et al., 2010) also showed that the phase transition was realized by the formation and growth of self-organized multiple macroscopic domains due to thermo-mechanical coupling, which strongly depended on loading rate (nominal strain rate $\dot{\varepsilon}$). The higher the strain rate, the larger the domain number and the smaller the domain spacing in the specimen.

The basic phenomena of the self-organized multiple-domain formation in a superelastic polycrystalline NiTi strip of a gauge length $L = 30$ mm (Zhang et al., 2010) at a nominal tensile strain rate $\dot{\varepsilon} = 3.3 \times 10^{-3}$/s can be illustrated by Fig. 1. After an initial near elastic loading, two high-strain domains (one near the top and the other near the bottom tapered end) nucleated simultaneously with a stress drop (see patterns *a* and *b* in Fig. 1). An instantaneous local heating of the domains due to the released latent heat can be detected by a thermal camera. In the subsequent growth of the two domains under continued stretching, the two fronts near the strip's tapered ends were soon arrested, which led to the speeding up of the other two fronts and a further temperature rise there. The increase in the front temperature in turn caused an increase in the applied stress to drive the fronts (*b*–*c* in Fig. 1(a)). When the applied stress reached the nucleation stress for the middle cooler untransformed region of the specimen, two new domains nucleated sequentially with stress drops (see *c*–*d* and *e*–*f* in Fig. 1). The subsequent propagation of the six fronts (*f*–*g* in Fig. 1(a) and (b)) was still accompanied by an increase in the front temperature, therefore the applied stress increased up to 413 MPa when the fifth domain nucleated (see *g*–*h* in Fig. 1). Because of the domain growth and heat conduction, the temperature of the specimen became more or less uniform and was higher than the initial temperature. The propagation stress for the fronts kept

* Corresponding author. Tel.: +852 23588655; fax: +852 23581543.
E-mail address: meqpsun@ust.hk (Q.P. Sun).

0020-7683/$ - see front matter © 2010 Elsevier Ltd. All rights reserved.
doi:10.1016/j.ijsolstr.2010.06.006

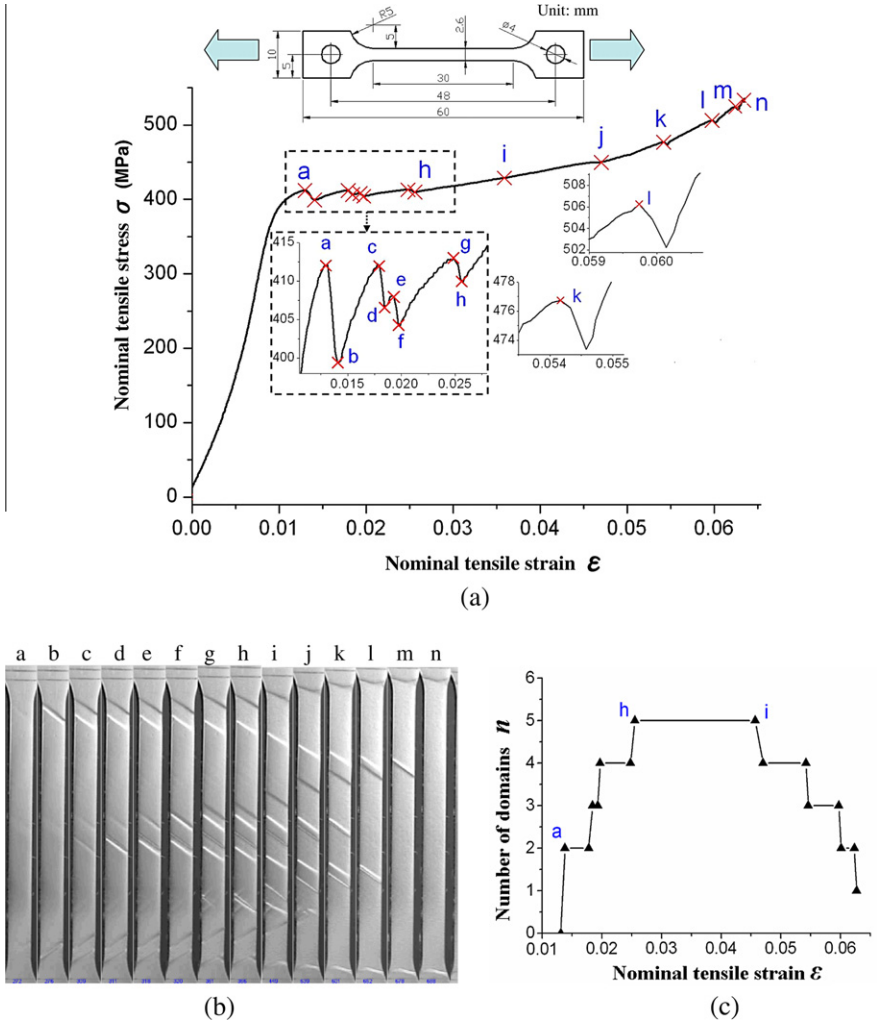

Fig. 1. Multiple-domain nucleation and growth in a NiTi strip under mechanical stretching at the nominal strain rate of 3.3×10^{-3}/s: (a) the nominal stress–strain response; (b) surface morphology; (c) variation in domain number n with the nominal strain.

increasing with loading but was no longer higher than the nucleation stress of the warmed austenite, so there was no further domain-nucleation in the continued stretching. Thus, the maximum number (n_{max}) of martensite domains in this loading process under the strain rate 3.3×10^{-3}/s was five (i.e., $n_{max} = 5$, see Fig. 1(c)). With further loading, the domains started to merge sequentially (see *j*–*m* in Fig. 1). Each merging was accompanied by a small stress drop and a reduction in domain number.

The rate dependence of the above self-organized domain patterns studied in a recent experiment (Zhang et al., 2010) is summarized in Fig. 2. It is seen from Fig. 2(a) that, for each strain rate, the number of martensite domains first increases with the nominal strain to reach a maximum (n_{max}) and then decreases due to domain merging. The maximum domain number n_{max} (or the minimum domain spacing $B_{min} = L/n_{max}$) increases (or decreases) nonlinearly with increasing strain rate as shown in Fig. 2(b) and (c). The typical domain patterns at a fixed nominal strain ($\varepsilon = 3.0\%$, which corresponds to roughly 60% transformation of the specimen gauge section) under different strain rates are shown in Fig. 2(d); it is seen that the higher the strain rate, the finer the domain patterns (i.e., more domains with smaller domain spacing).

The basic physics behind the rate dependence of the domain spacing is that, under a given stretching rate, the local self-heating of the domain-fronts causes an increase in the applied stress for domain-front propagation (Leo et al., 1993; Bruno et al., 1995; Shaw and Kyriakides, 1995; Shaw and Kyriakides, 1997); as long as this stress is higher than the domain-nucleation stress at the coolest point of the untransformed region, new domains will nucleate. Such nucleation will repeatedly take place until there are sufficient domains in the specimen so that the above nucleation criterion is violated. As a result, for each stretching rate, there exists a maximum domain number n_{max} (or minimum domain spacing B_{min}). In principle, the higher the stretching rate, the less time to transfer the latent heat and therefore the more domains we observe. Based on the above scenario of thermo-mechanical coupling, computational studies were performed (Shaw and Kyriakides, 1998; Shaw, 2000; Iadicola and Shaw, 2004) and important insight into the multiple-domain formations has been obtained. Generally speaking, the processes of the domain formation and evolution under stretching involve multiple mechanical instabilities with complicated transient heat transfer and multiple moving heat sources. The mathematical skills involved in solving the coupled governing equations are very demanding. Analytical expression of the rate dependence of domain spacing (an emerging length scale of the deformation patterns) has not been attempted so far.

The objective of this paper is, using a simple analytical model rather than complicated instability analysis and computational simulations, to quantify the roles of the material's thermal and mechanical properties, heat transfer boundary condition and the

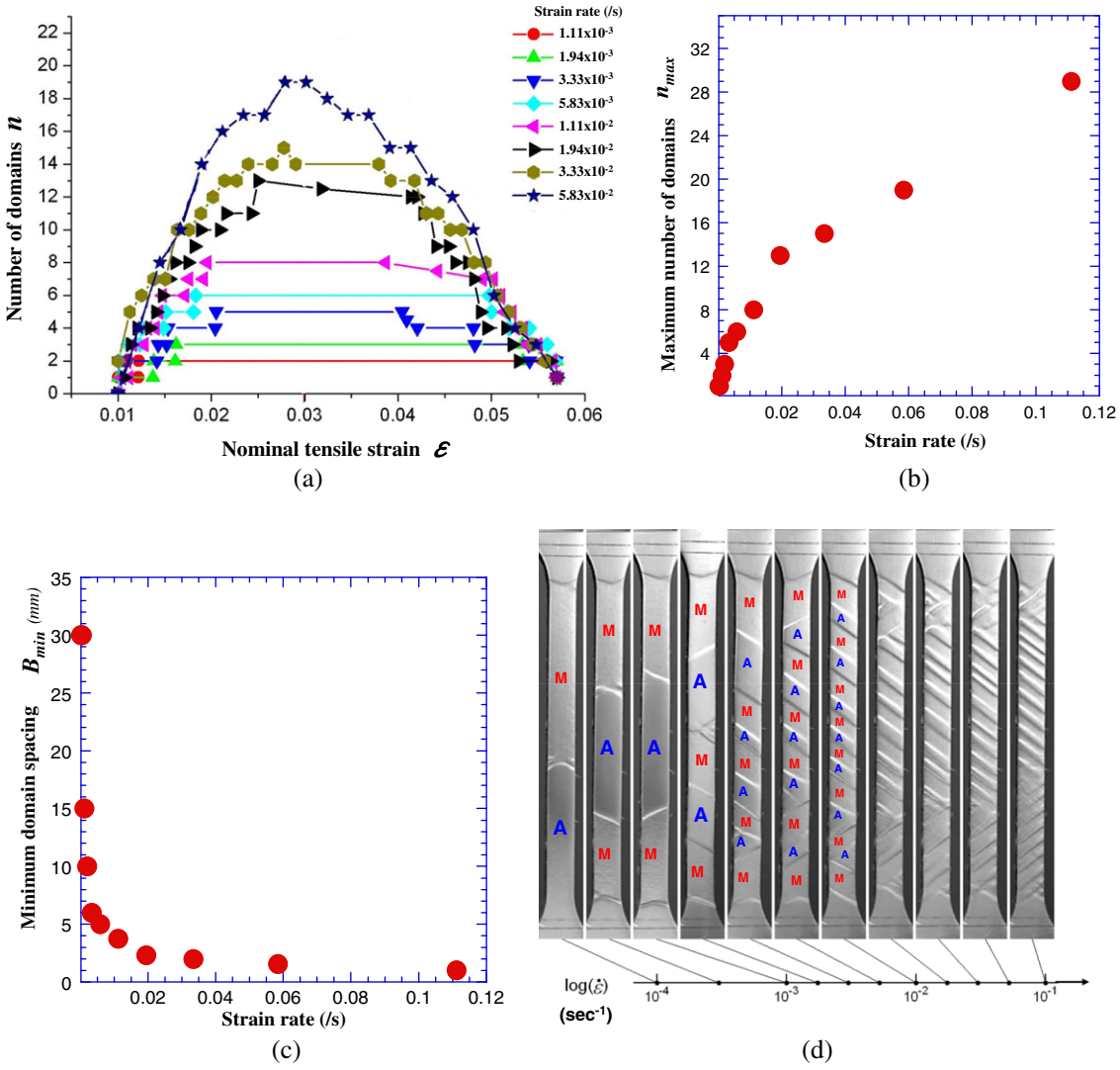

Fig. 2. (a) Variation in the number of domains with the applied nominal strain at different strain rates; (b) variation in maximum domain number n_{max} with the applied strain rate; (c) variation in minimum domain spacing B_{min} with the applied strain rate; (d) domain patterns at a fixed nominal strain of 3% under different strain rates.

external loading rate (i.e., the rate of phase transformation and latent heat release) in the observed domain spacing in the NiTi strip. The remaining parts of this paper are organized as follows: Section 2 describes the thermo-mechanical material properties, based on which a criterion for domain-nucleation in the multiple-domain configuration with non-uniform temperature distributions is proposed. In Section 3, the theoretical predictions on the rate-dependent maximum domain number n_{max} and minimum domain spacing B_{min} are obtained and compared with the experimental observations. Conclusions are given in Section 4.

2. Theoretical model

To quantify the effects of the thermo-mechanical coupling on the rate-dependent domain formation, our model basically consists of three components: (1) temperature dependence of the material's transformation stresses; (2) temperature profile of a single propagating domain-front (moving heat source); and (3) criterion of domain-nucleation in non-uniform temperature field of a multiple-domain configuration. Based on the three components, the rate-dependent maximum domain number n_{max} and the minimum domain spacing B_{min} are derived in this section.

2.1. Temperature dependence of transformation stress

From the existing theories and experiments (Leo et al., 1993; Shaw and Kyriakides, 1997; Brinson et al., 2004), the stress-induced phase transition behavior of the fine-grained polycrystalline NiTi in quasi-one-dimensional (1D) structures (wires and strips) under isothermal tensile loading can be characterized (Fig. 3(a)) by a macroscopic domain-nucleation stress σ_N (i.e., the peak stress) and a domain-front propagation stress σ_P (i.e., the plateau stress), with $\Delta\sigma$ being the difference between σ_N and σ_P (i.e., the stress drop in the domain-nucleation). For simplicity, $\Delta\sigma$ is taken as a material constant for the given strip geometry. The temperature dependence of σ_N and σ_P can be approximated by linear functions of temperature θ as (Fig. 3(b)):

$$\sigma_P(\theta) = \sigma_0 + b\cdot(\theta-\theta_0) \tag{1a}$$

$$\sigma_N(\theta) = \sigma_P(\theta) + \Delta\sigma = \sigma_0 + b\cdot(\theta-\theta_0) + \Delta\sigma \tag{1b}$$

where θ_0 is the ambient temperature (here the initial temperature of the specimen is equal to the ambient temperature θ_0); σ_0 is the plateau stress at temperature θ_0; b (>0) is the coefficient of the temperature dependence. Eq. (1) means that, the higher the tempera-

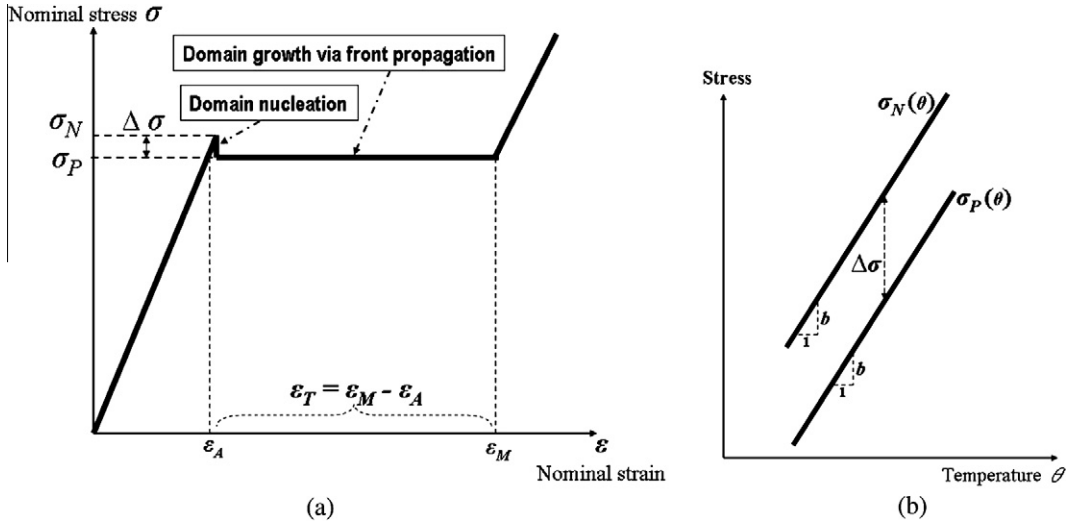

Fig. 3. (a) Schematic isothermal stress–strain curve; (b) temperature dependence of domain-nucleation stress and front propagation stress.

ture, the higher the applied stresses needed for the macroscopic domain-nucleation and domain growth.

From experiments such as in Fig. 1, it is well noted that there is homogeneous transformation in the specimen before the beginning of the localization (macroscopic domain-nucleation at point "*a*" in Fig. 1). Such homogeneous transformation releases small amount of heat to increase the specimen's temperature homogeneously (Brinson et al., 2004; Favier et al., 2007). As will be shown in next sections, it is the local temperature rise at the macroscopic domain-fronts, instead of the initial uniform heating, that governs the formation of multiple-domains. So, the heat effect of the homogeneous transformation is neglected in present model for simplicity.

2.2. Temperature field around a single propagating domain-front

To simplify the description of the temperature field of the NiTi strip containing a single propagating front during the phase transformation, we model the strip as a 1D rod of a length L and an effective radius r (here the radius r is of the same order of the strip's thickness). The temperature field $\theta(x,t)$ of the 1D rod is governed by the heat convection–conduction equation (Bruno et al., 1995) and Stefan condition at the domain-front:

$$\lambda \cdot \frac{\partial \theta}{\partial t} = k \cdot \frac{\partial^2 \theta}{\partial x^2} - \frac{2h}{r}(\theta - \theta_0) \tag{2a}$$

$$\left[k \cdot \frac{\partial \theta}{\partial x}\right]_-^+ = -l \cdot v \tag{2b}$$

where x denotes the axial coordinate of the rod and t denotes the time coordinate; λ, k, h, v and l are, respectively, the heat capacity per unit volume, heat conductivity, coefficient of heat convection between the specimen and the environment (air), front propagation velocity, and the released latent heat per unit volume during phase transformation; $[A]_-^+$ denotes the jump of quantity A across the front, i.e., $[A]_-^+ = A_+ - A_-$. Strictly speaking, the material properties λ and k depend on the phase state — austenite or martensite (Amalraj et al., 2000) and Eq. (2) should be formulated with different material parameters for the two phases in a multi-domain configuration. For the purpose of simplicity and without losing the key features, we assume that λ and k have the same values in both phases, i.e., the bar has uniform properties (heat capacity and heat conductivity) and Eq. (2) is valid for the whole specimen.

For a single steady-state propagating front in an infinitely long rod (Bruno et al., 1995), the solution of Eq. (2) gives the temperature field ahead of the propagating front which serves as the origin of the moving coordinate y (see Fig. 4):

$$\theta(y) = \theta_0 + \theta_h \cdot e^{-\frac{\lambda \cdot v}{2k}\left[1+\sqrt{1+D}\right]\cdot y}$$

$$\text{where} \quad \theta_h = \frac{l}{\lambda\sqrt{1+D}} \quad \text{and} \quad D = \frac{8h \cdot k}{r \cdot \lambda^2 \cdot v^2} \tag{3}$$

θ_h is the temperature increase at the front with propagation velocity v. y (>0) denotes the distance ahead of the moving front (Fig. 4). Due to the released latent heat, the front temperature θ_{front} is equal to $\theta_0 + \theta_h$. It is seen that the magnitude of the temperature rise (θ_h) depends on the material's thermal properties (λ, k and l), specimen size (radius r), heat transfer boundary condition (i.e., heat convection coefficient h) and the domain-front propagation velocity v which is related to the external loading rate $\dot{\varepsilon}$ and the number of the propagating domain-fronts.

As shown in Fig. 4, the temperature decays exponentially with the distance y from the domain-front which has the highest temperature. In other words, the untransformed material (austenite) far from the front has a much lower temperature than that near the front. So, under a quasi-static stretching (no inertial force), the material away from the front is easier to be transformed due to its lower transformation stress (Eq. (1)).

2.3. Domain-nucleation criterion in non-isothermal multi-domain configuration

If the specimen has a uniform temperature (e.g., isothermal stretching under uniform stress field), the stress σ_N to nucleate a domain is always larger than the stress σ_P to move the domain-front (propagating interface) (Eq. (1) and Fig. 3). Therefore, the specimen under an isothermal displacement-controlled stretching deforms via the nucleation and growth of a single domain with two propagating fronts.

In most real situations, due to the released heat and heat transfer, the specimen's temperature is non-uniform (see Eq. (3) and Fig. 4). The increase in the front's temperature ($\theta_0 + \theta_h$) leads to an increase in the applied stress to drive the hot fronts (Eq. (1)). When the applied stress is larger than the domain-nucleation stress of the coolest location in the austenite region, a new martensite domain will nucleate there. Then, the specimen's deformation will adopt the mode of multiple-domain growth. In formulating the criterion of domain nucleation and front propagation in the non-uniform temperature field, we have used the following approximations:

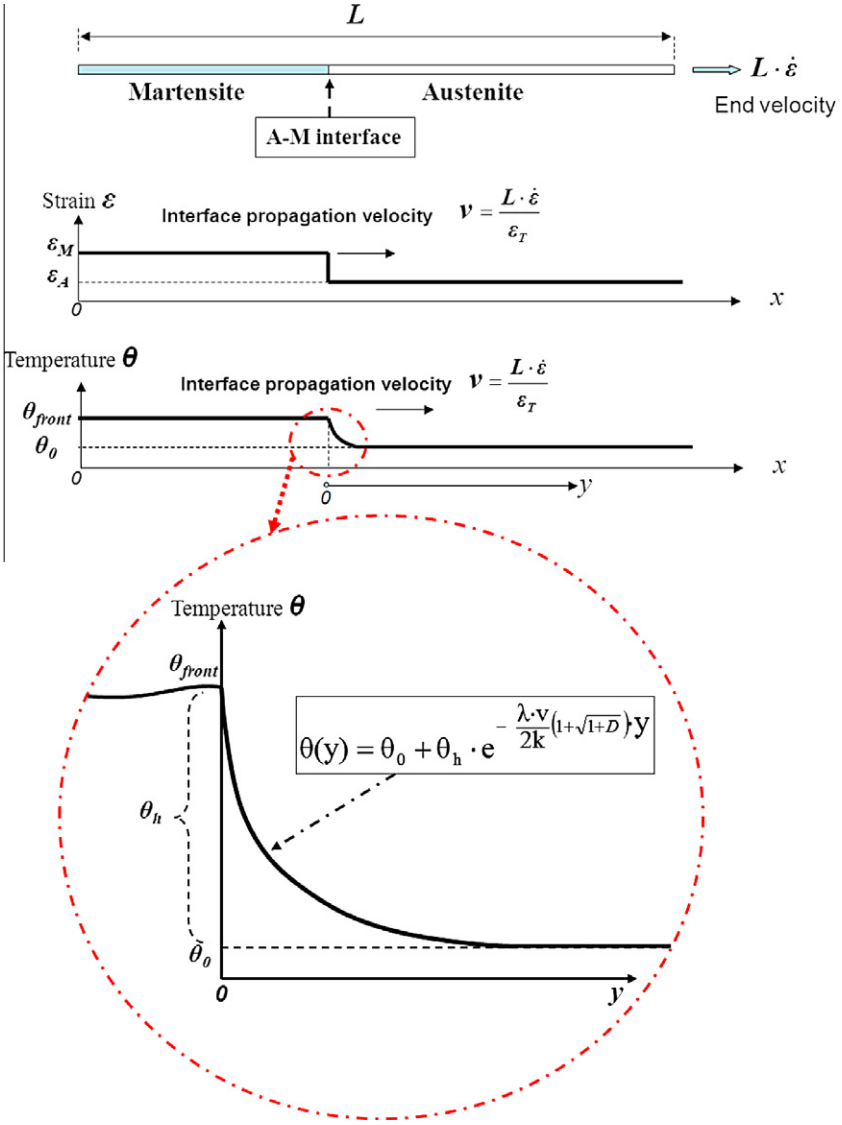

Fig. 4. Distributions of strain and temperature for a steady-state single propagating domain-front in a 1D rod stretched at nominal strain rate $\dot{\varepsilon}$.

(1) As shown in Fig. 2(d), the multiple-domains can be considered as uniformly distributed over the specimen.
(2) As observed in experiment (Zhang et al., 2010; Feng et al., 2009), the multiple-domain formation take place in a time period much shorter than the whole loading time, and therefore can be approximated as instantaneous self-organized formation as schematically shown in Fig. 5. The thermal interaction between the just nucleated neighboring domain fronts can be ignored at the stage of multiple domain nucleations and Eq. (3) is still a good approximation for the temperature profile of each domain-front (see Fig. 5).
(3) From experimental observations (Shaw and Kyriakides, 1995; Shaw and Kyriakides, 1997; Zhang et al., 2010), the $2n$ propagating fronts of n domains have more or less the same velocity, so we can calculate the front velocity v as

$$v = \frac{L \cdot \dot{\varepsilon}}{2 \cdot n \cdot \varepsilon_T} \tag{4}$$

where $\varepsilon_T = \varepsilon_M - \varepsilon_A$ is the characteristic austenite–martensite transformation strain of the material (Fig. 3(a)).

To keep the fronts propagating, the applied stress $\sigma_{applied}$ on the specimen must satisfy

$$\sigma_{applied} = \sigma_P(\theta_{front}) \tag{5a}$$

With Eqs. (1a) and (3), Eq. (5a) becomes

$$\sigma_{applied} = \sigma_0 + b \cdot (\theta_{front} - \theta_0) = \sigma_0 + b \cdot \frac{l}{\lambda\sqrt{1+D}} = \sigma_0 + b \cdot \frac{l}{\lambda\sqrt{1+\frac{8h \cdot k}{r \cdot \lambda^2 \cdot v^2}}} \tag{5b}$$

It is seen that the required stress for the front propagation nonlinearly depends on λ, h, k, r and v (v is related to domain number n and strain rate $\dot{\varepsilon}$).

Under quasi-static loading (no inertia effect), the stress field of the bar is uniform (i.e., all parts of the specimen are under the same stress $\sigma_{applied}$ due to mechanical equilibrium). New domains will nucleate at the coolest point of the untransformed region (Fig. 5) when $\sigma_{applied}$ satisfy:

$$\sigma_{applied} \geqslant \sigma_N(\theta_{coolest}) \tag{5c}$$

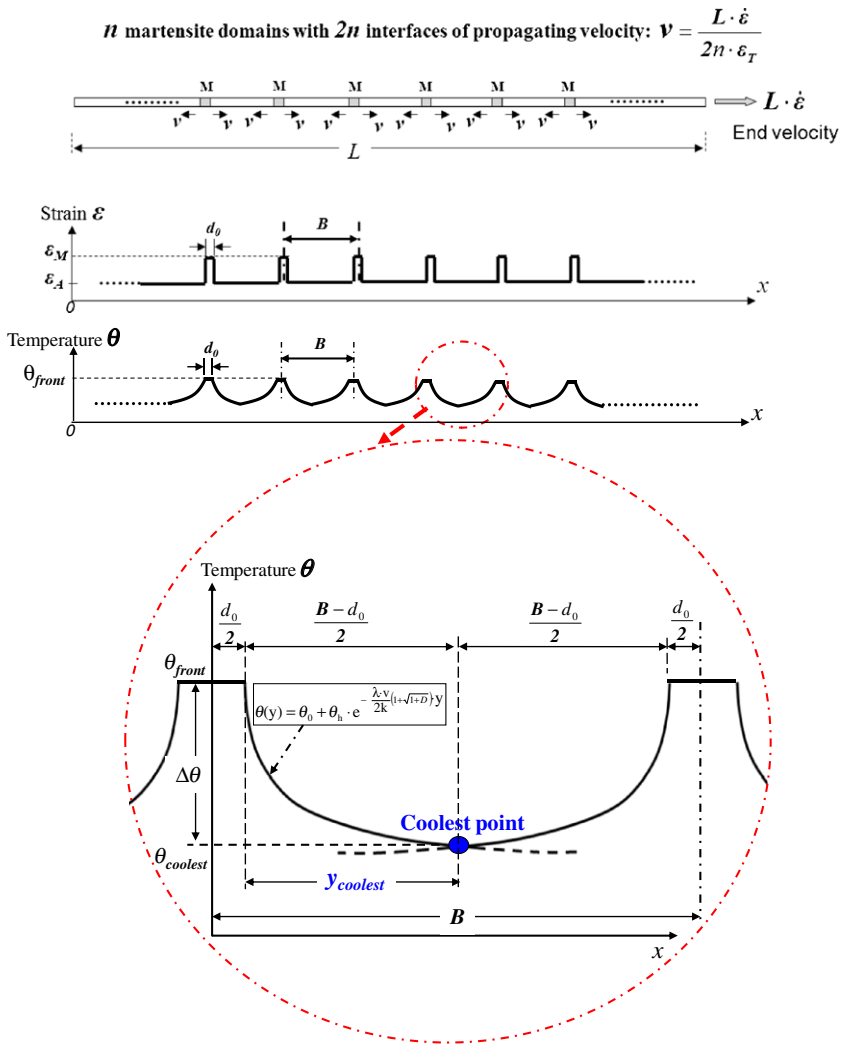

Fig. 5. Distributions of strain and temperature for multiple-domains in a stretched 1D rod at nominal strain rate $\dot{\varepsilon}$.

Using Eq. (1b), Eq. (5c) becomes

$$\sigma_{applied} \geqslant \sigma_0 + b \cdot (\theta_{coolest} - \theta_0) + \Delta\sigma \tag{5d}$$

Based on Eqs. (5b) and (5d), the above stress criterion can be expressed as a temperature criterion of domain-nucleation in the multiple-domain configuration:

$$\Delta\theta \geqslant \Delta\theta_{critical} \tag{6a}$$

where

$$\Delta\theta \equiv \theta_{front} - \theta_{coolest} \tag{6b}$$

$$\Delta\theta_{critical} \equiv \frac{\Delta\sigma}{b} \tag{6c}$$

Eq. (6a) means that new domain will nucleate as long as $\Delta\theta$ in the specimen is larger than the critical value $\Delta\theta_{critical}$ (see Fig. 5).

2.4. Rate dependence of n_{max} and B_{min}

With the increase in the domain number n and therefore the decrease in domain spacing B (=L/n), the value of $\theta_{coolest}$ increases (i.e., the untransformed coolest point is getting closer to the hot fronts and therefore becomes warmer). This makes $\Delta\theta$ (=$\theta_{front} - \theta_{coolest}$) decreases. At the same time, the velocity v of each front decreases with increasing n (Eq. (4)), leading to a decrease in the front's temperature θ_{front} (Eq. (3)) and therefore also causing a decrease in $\Delta\theta$. Eventually, when $\Delta\theta$ is decreased below the critical value $\Delta\theta_{critical}$, no domain will nucleate according to Eq. (6a). Thus, we have the critical condition

$$\Delta\theta = \Delta\theta_{critical} \tag{6d}$$

which corresponds to the instant when the domain number in the specimen reaches a maximum ($n_{\max}$). As shown in Fig. 5, the distance between a hot front and its neighboring coolest point is denoted by $y_{coolest}$:

$$y_{coolest} = \frac{B - d_0}{2} \approx \frac{B}{2} = \frac{L}{2n} \tag{7}$$

where d_0 is the thickness of a just nucleated domain, which is usually much smaller than the domain spacing (i.e., $d_0 \ll B$). Substituting Eq. (3) into Eq. (6d), we obtain

$$1 - e^{-\frac{\lambda}{2k}\left[v + \sqrt{v^2 + \frac{8h\cdot k}{r\cdot\lambda^2}}\right]\cdot y_{coolest}} = \frac{\Delta\theta_{critical}}{\theta_h} \tag{8a}$$

Substituting v (Eq. (4)), $y_{coolest}$ (Eq. (7)), θ_h (Eq. (3)) and $\Delta\theta_{critical}$ (Eq. (6c)) into Eq. (8a), the critical condition for the maximum domain number ($n_{\max}$) becomes

$$D_2 \cdot \frac{\dot{\varepsilon}}{n_{\max}^2} \cdot \left[1 + \sqrt{1 + D_1 \cdot \left(\frac{n_{\max}}{\dot{\varepsilon}}\right)^2}\right] = -\ln\left(1 - D_3\sqrt{1 + D_1 \cdot \left(\frac{n_{\max}}{\dot{\varepsilon}}\right)^2}\right) \tag{8b}$$

where $D_1 = \frac{32h\cdot k\cdot \varepsilon_T^2}{r\cdot \lambda^2\cdot L^2}$, $D_2 = \frac{\lambda\cdot L^2}{8k\cdot \varepsilon_T}$, $D_3 = \frac{\lambda\cdot \Delta\theta_{critical}}{l} = \frac{\lambda\cdot\Delta\sigma}{l\cdot b}$.

Eq. (8b) shows a nonlinear dependence of the maximum domain number n_{max} on the strain rate $\dot{\varepsilon}$, in which $D_1 \sim D_3$ are constants representing the combined effects of the material properties, specimen geometry and the environmental condition (heat convection coefficient h).

Eq. (8b) contains a transcendental function (*logarithmic function*) which cannot be analytically solved to explicitly express n_{max} in terms of $\dot{\varepsilon}$ and $D_1 \sim D_3$. The $n_{max} \sim \dot{\varepsilon}$ relation has to be numerically calculated for the real NiTi material properties and the specimen geometry (Table 1). The theoretical calculations of the $n_{max} \sim \dot{\varepsilon}$ relation for different values of h (heat convection coefficient) are shown in Fig. 6. It is seen that, for each given h, the maximum domain number n_{max} increases with increasing nominal strain rate $\dot{\varepsilon}$; this is because the higher the strain rate, the faster the release of heat, and the higher the temperature rise at the propagating fronts and therefore more domain-nucleations. Furthermore, at each given strain rate, n_{max} decreases with increase in the heat convection (increasing h); this is because the higher the h, the faster the transfer of heat to the environment and therefore the more effective reduction of the front temperature. In addition to the above general trend, we will discuss the following two cases which have explicit analytical solutions and are more relevant to the domain spacing in real experimental conditions.

It should be noticed that the above 1D model is valid for the tensile tests of NiTi thin wires and long slim strips where the stress state of the materials is close to a simple tensile stress state. For other complex structures (e.g., square plates and tubes), the stress state is more complex (He and Sun, 2009a; He and Sun, 2010) and the 1D model is not suitable for the description of the domain patterns in 2D or 3D structures.

Table 1
Material properties and specimen geometry in the experiment (Zhang et al., 2010).

Property	Symbol	Value	Unit
Latent heat	l	96.8	MPa
Heat capacity	λ	3.2×10^6	J/(m^3 K)
Heat conductivity	K	18.3	W/(m K)
A–M transformation strain	ε_T	4.8%	
Isothermal stress drop	$\Delta\sigma$	18	MPa
Temperature coefficient of transformation stress	b	5.7	MPa/K
Heat convection coefficient (stagnant air)	h	6.5	W/(m^2 K)
Specimen length	L	30	mm
Effective radius of rod (half strip's thickness)	r	0.25	mm

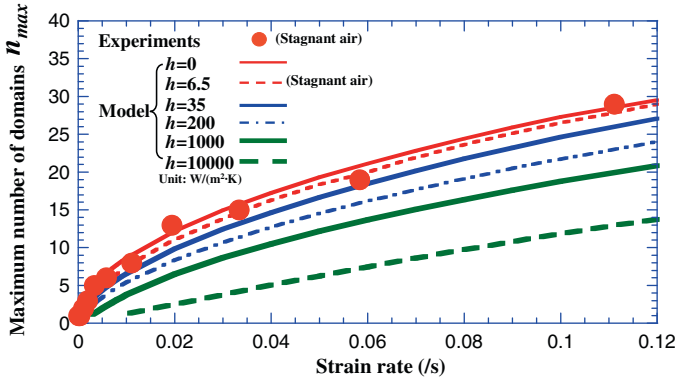

Fig. 6. Comparison between the numerical calculations of the maximum domain number n_{max} and the experimental observations.

3. Discussion and comparison with the experiments in stagnant air

Compared with the test in stagnant water (h = 890 W/(m^2 K)), the heat convection in stagnant air is weak with a very low convective heat transfer coefficient ($h \approx 6.5$ W/(m^2 K), see Leo et al., 1993; Bruno et al., 1995; Holman, 2010). As shown in Fig. 6, the theoretical calculation of the $n_{max} \sim \dot{\varepsilon}$ relation with h = 6.5 W/(m^2 K) agrees well quantitatively with the experiments of NiTi strips in stagnant air (Zhang et al., 2010). To have a better understanding of this, we consider the following two extreme cases for which there are explicit analytical solutions.

3.1. Domain spacing in extremely weak heat convection (h = 0)

We consider the extreme case of h = 0 where the effect of heat convection is ignorable. From Eq. (8b), we can obtain an explicit power-law scaling on the strain rate ($\dot{\varepsilon}$) dependence of n_{max} as

$$n_{max} = \sqrt{\frac{2D_2\cdot\dot{\varepsilon}}{-\ln(1-D_3)}} = C\cdot L\cdot(\dot{\varepsilon})^{\frac{1}{2}}$$
$$\text{where}\quad C = \sqrt{\frac{\lambda}{-4k\cdot\varepsilon_T\cdot\ln\left(1-\frac{\Delta\theta_{critical}\cdot\lambda}{l}\right)}} \tag{9}$$

In this extreme case, the roles of the thermo-mechanical properties of the material ($\lambda, k, \varepsilon_T, \Delta\theta_{critical}$ and l) in controlling the domain number n_{max} (or number density n_{max}/L) are included in the term C. Eq. (9) is plotted in Fig. 6 as an upper limit curve. It is seen that the theoretical prediction with h = 0 (ignoring the heat convection) well approximates the real situation in stagnant air ($h \approx 6.5$ W/(m^2 K)). It is also worth mentioning that, in the recent numerical simulation by Iadicola and Shaw, 2004 on the rate-dependent maximum domain number in NiTi, a power-law relationship with an exponent 0.58 was obtained by fitting the computational results. This relationship is close to the present analytical result of the exponent 0.5 in Eq. (9).

From Eq. (9), the strain rate dependence of the minimum domain spacing B_{min} can be immediately expressed as the following power-law form:

$$B_{min} \equiv \frac{L}{n_{max}} = \frac{1}{C\cdot\sqrt{\dot{\varepsilon}}} = \frac{1}{C}\cdot(\dot{\varepsilon})^{-\frac{1}{2}} \tag{10}$$

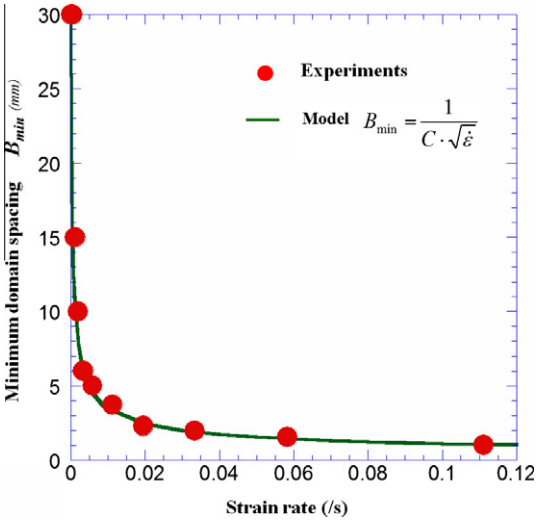

Fig. 7. Comparison between the experimental observations (in stagnant air) and the theoretical (power-law) predictions on the minimum domain spacing B_{min}.

As shown in Fig. 7, the prediction of Eq. (10) agrees well with the experimental data without any fitting parameters. From both Figs. 6 and 7 we can see that, when the heat convection between the specimen and the environment is weak such as in stagnant air, the above simple power-law scaling gives a good description on the rate-dependent domain number and domain spacing.

3.2. Domain spacing in extremely strong heat convection (very large h)

When h becomes very large, the second term on the left-hand side of Eq. (8a) approaches zero; we have

$$1 = \frac{\Delta\theta_{critical}}{\theta_h} \tag{11a}$$

Substituting Eqs. (3) and (4) into (11a), we obtain a linear relationship between $n_{\max}$ and $\dot{\varepsilon}$ (see the result for $h = 10^4$ W/(m^2 K) in Fig. 6):

$$n_{max} = S \cdot \dot{\varepsilon} \tag{11b}$$

where the slope S is

$$S = L \cdot H, \quad \text{where} \quad H = \frac{l}{4\Delta\theta_{critical} \cdot \varepsilon_T} \cdot \sqrt{\frac{r}{2h \cdot k}} \tag{11c}$$

It is seen that the slope S will decrease to zero as $h \to \infty$. That means the deformation pattern is not sensitive to the strain rate ($S \to 0$) because the strong heat transfer ($h \to \infty$) can always bring the bar's temperature very close to the ambient temperature (i.e., isothermal condition). This conclusion is consistent with the many experimental observation (e.g., see Grabe and Bruhns, 2008; He et al., 2010) that there is no rate dependence of the material's responses in isothermal condition.

Based on Eqs. (11b) and (11c) for large h, the minimum domain spacing $B_{\min}$ is inversely proportional to the strain rate as

$$B_{\min} \equiv \frac{L}{n_{\max}} = \frac{1}{H \cdot \dot{\varepsilon}} = \frac{1}{H} \cdot (\dot{\varepsilon})^{-1} \tag{12}$$

Finally it should be noticed that, besides heat convection, heat conduction has effect on domain spacing. From both Eqs. (9) and (11c), it is seen that the domain number decreases with increasing heat conductivity k. Moreover, specimen geometry (e.g., radius r) not only affects the heat convection (Eq. (2a)), but also governs the thickness of the macro-domain front (He and Sun, 2009b). These issues remain to be studied in the future.

4. Conclusions

The domain spacing, as an emerging length scale of the observed self-organized domain patterns in the polycrystalline NiTi strip under non-isothermal stretching, is determined by the strong coupling between the material's nonlinear mechanical behavior and the transfer of the latent heat. In the coupling, the competition among the different time scales of loading (by strain rate $\dot{\varepsilon}$, also the time scale of heat release), heat conduction (conductivity k) and convection (convective coefficient h) plays an important role. Based on a simplified one-dimensional model, we have attempted to reveal the roles of $\dot{\varepsilon}$, k and h in controlling the domain number and spacing. For most NiTi polycrystals and heat transfer boundary conditions, the maximum domain number $n_{\max}$ (minimum domain spacing $B_{\min}$) increases (decreases) with increasing applied nominal strain rate $\dot{\varepsilon}$; and decreases (increases) with increasing heat convection (h) and conductivity (k).

In addition to the above general trends, we have obtained simple explicit analytical expressions for the rate dependence of domain spacing for the following two cases (i.e., in conduction dominated and convection dominated regions):

- For the case of $h = 0$ (no convection, i.e., conduction is the only mechanism of the heat transfer), a simple power-law scaling relationship (with exponent -0.5) between the domain spacing and strain rate is obtained, which agrees quantitatively well with the experimental data in stagnant air without any fitting parameters.
- For the case of very large h (i.e., convection plays a dominant role in the domain spacing), the domain spacing is inversely proportional to the strain rate. This remains to be confirmed by future experiments.

Acknowledgements

The financial support from the Hong Kong Research Grants Council under a CERG grant (GRF Project No. 620109) is gratefully acknowledged.

References

Abeyaratne, R., Knowles, J.K., 1993. A continuum model of a thermoelastic solid capable of undergoing phase transitions. J. Mech. Phys. Solids 41, 541–571.
Amalraj, J.J., Bhattacharyya, A., Faulkner, M.G., 2000. Finite-element modeling of phase transformation in shape memory alloy wires with variable material properties. Smart Mater. Struct. 9, 622–631.
Bruno, O.P., Leo, P.H., Reitich, F., 1995. Free boundary conditions at austenite–martensite interfaces. Phys. Rev. Lett. 74, 746–749.
Brinson, L.C., Schmidt, I., Lammering, R., 2004. Stress-induced transformation behavior of a polycrystalline NiTi shape memory alloy: micro and macro-mechanical investigations via in situ optical microscopy. J. Mech. Phys. Solids 52, 1549–1571.
Churchill, C.B., Shaw, J.A., Iadicola, M.A., 2009. Tips and tricks for characterization shape memory alloy wire: Part 3: localization and propagation phenomena. Exp. Tech. 33, 70–78.
Delaey, L., Krishnan, R.V., Tas, H., Warlimont, H., 1974. Review thermoelasticity, pseudoelasticity and the memory effects associated with martensitic transformations, Part 1. Structural and microstructural changes associated with transformations. J. Mater. Sci. 9, 1521–1535.
Favier, D., Louche, H., Schlosser, P., Orge'as, L., Vacher, P., Debove, L., 2007. Homogeneous and heterogeneous deformation mechanisms in an austenitic polycrystalline Ti – 50.8 at.% Ni thin tube under tension. Investigation via temperature and strain fields measurements. Acta Mater. 55, 5310–5322.
Feng, P., Sun, Q.P., 2006. Experimental investigation on macroscopic domain formation and evolution in polycrystalline NiTi microtubing under mechanical force. J. Mech. Phys. Solids 54, 1568–1603.
Feng, P., He, Y.J., Sun, Q.P., in press. Strain rate effects on morphology and temperature evolution of NiTi shape memory alloys strips subject to uniaxial tensile loading. In: Proceeding of 20th International Conference on Adaptive structure and Technologies.
Grabe, C., Bruhns, O.T., 2008. On the viscous and strain rate dependent behavior of polycrystalline NiTi. Int. J. Solids Struct. 45, 1876–1895.
He, Y.J., Sun, Q.P., 2009a. Effects of structural and material length scales on stress-induced martensite macro-domain patterns in tube configurations. Int. J. Solids Struct. 46, 3045–3060.
He, Y.J., Sun, Q.P., 2009b. Scaling relationship on macroscopic helical domains in NiTi tubes. Int. J. Solids Struct. 46, 4242–4251.
He, Y.J., Sun, Q.P., 2010. Macroscopic equilibrium domain structure and geometric compatibility in elastic phase transition of thin plates. Int. J. Mech. Sci. 52, 198–211.
He, Y.J., Yin, H., Zhou, R.H., Sun, Q.P., 2010. Ambient effect on damping peak of NiTi shape memory alloy. Mater. Lett. 64, 1483–1486.
Holman, J.P., 2010. Heat Transfer, 10th ed. The Mcgraw-Hill Companies. 10-11.
Iadicola, M.A., Shaw, J.A., 2004. Rate and thermal sensitivities of unstable transformation behavior in a shape memory alloy. Int. J. Plast. 20, 577–605.
Leo, P.H., Shield, T.W., Bruno, O.P., 1993. Transient heat transfer effects on the pseudoelastic behavior of shape-memory wires. Acta Metall. Mater. 41, 2477–2485.
Li, Z.Q., Sun, Q.P., 2002. The initiation and growth of macroscopic martensite band in nano-grained NiTi microtube under tension. Int. J. Plast. 18, 1481–1498.
Muller, I., Villaggio, P., 1977. A model for an elastic–plastic body. Arch. Ration. Mech. Anal. 65, 25–46.
Ng, K.L., Sun, Q.P., 2006. Stress-induced phase transformation and detwinning in NiTi tubes. Mech. Mater. 38, 41–56.
Pieczyska, E.A., Gadaj, S.P., Nowacki, W.K., Tobushi, H., 2004. Investigation of nucleation and propagation of phase transitions in TiNi SMA. QIRT J. 1, 117–128.
Pieczyska, E.A., Gadaj, S.P., Nowacki, W.K., 2006. Phase-transformation fronts evolution for stress- and strain- controlled tension tests in TiNi shape memory alloy. Exp. Mech. 46, 531–542.
Puglisi, G., Truskinovsky, L., 2005. Thermodynamics of rate-independent plasticity. J. Mech. Phys. Solids 53, 655–679.

Shaw, J.A., Churchill, C.B., Iadicola, M.A., 2008. Tips and tricks for characterization shape memory alloy wire: Part I — differential scanning calorimetry and basic phenomena. Exp. Tech., 55–62.

Shaw, J.A., Kyriakides, S., 1995. Thermo-mechanical aspects of NiTi. J. Mech. Phys. Solids 43, 1243–1281.

Shaw, J.A., Kyriakides, S., 1997. On the nucleation and propagation of phase transformation fronts in a NiTi alloy. Acta Mater. 45, 683–700.

Shaw, J.A., Kyriakides, S., 1998. Initiation and propagation of localized deformation in elasto-plastic strips under uniaxial tension. Int. J. Plast. 13, 837–871.

Shaw, J.A., 2000. Simulations of localized thermo-mechanical behavior in a NiTi shape memory alloy. Int. J. Plast. 16, 541–562.

Sun, Q.P., Li, Z.Q., 2002. Phase-transformation in superelastic NiTi polycrystalline microtubes under tension and torsion? From localization to homogeneous deformation. Int. J. Solids Struct. 39, 3797–3809.

Sun, Q.P., He, Y.J., 2008. A multiscale continuum model of the grain-size dependence of the stress hysteresis in shape memory alloy polycrystals. Int. J. Solids Struct. 45, 3868–3896.

Zhang, X.H., Feng, P., He, Y.J., Yu, T.X., Sun, Q.P., 2010. Rate dependence of macroscopic domain patterns in stretched NiTi strips. Int. J. Mech. Sci., submitted for publication.